Mechanism for Anomalous Hall Ferromagnetism in Twisted Bilayer Graphene

Nick Bultinck,[1,*] Shubhayu Chatterjee,[1,*] and Michael P. Zaletel[1,2]
[1]Department of Physics, University of California, Berkeley, California 94720, USA
[2]Materials Sciences Division, Lawrence Berkeley National Laboratory, Berkeley, California 94720, USA

(Received 20 February 2019; accepted 1 April 2020; published 21 April 2020)

Motivated by the recent observation of an anomalous Hall effect in twisted bilayer graphene, we use a lowest Landau level model to understand the origin of the underlying symmetry-broken correlated state. This effective model is rooted in the occurrence of Chern bands which arise due to the coupling between the graphene device and its encapsulating substrate. Our model exhibits a phase transition from a spin-valley polarized insulator to a partial or fully valley unpolarized metal as the bandwidth is increased relative to the interaction strength, consistent with experimental observations. In sharp contrast to standard quantum Hall ferromagnetism, the Chern number structure of the flat bands precludes an instability to an intervalley coherent phase, but allows for an excitonic vortex lattice at large interaction anisotropy.

DOI: 10.1103/PhysRevLett.124.166601

Moiré graphene systems are a class of simple van der Waals heterostructures [1] hosting interaction driven low-energy physics, making them an exciting platform to advance our understanding of correlated quantum matter. In twisted bilayer graphene (TBG) with a small twist angle between adjacent layers, interaction effects are enhanced by van Hove singularities coming from eight nearly flat bands around charge neutrality (CN) in the Moiré- or mini-Brillouin zone (MBZ) [2–21]. Observation of correlated insulating states when 2 or 6 of the 8 TBG flat bands are filled confirms the importance of interactions [22–28].

Recent experiments indicate that certain magic angle graphene devices have large resistance peaks at $\nu = 0, 3$, with the latter featuring an anomalous Hall (AH) effect detected via hysteresis in the Hall conductance as a function of the out-of-plane magnetic field [29]. The Hall conductance is of order e^2/h but not yet quantized. Some have detected an meV-scale gap at CN, and a hysteretic behavior of the Hall conductance with applied field at $\nu = -1$ [30]. In this Letter we discuss how the breaking of the 180° rotational symmetry (C_{2z}) by a partially aligned hexagonal boron-nitride (h-BN) substrate could explain these observations. A variety of works [31–37] have found that h-BN opens up a band gap at the Dirac points of graphene whose magnitude depends on the graphene and h-BN alignment angle, reaching $\Delta_{AB} \sim$ 17 meV [37] to ∼30 meV [35,36] at perfect alignment. Notably, even in seemingly unaligned devices with little or no observable h-BN induced Moiré potential, band gaps of several meV are still observed [36,37]. In TBG, the substrate can likewise gap out the band Dirac points at the $K_\pm$ points of the MBZ, splitting the bands as $8 = 4 + 4$ to create a gap at CN. We find that for certain sublattice splittings the resulting flat bands have Chern number $C = \pm 1$. This makes the TBG case similar to ABC stacked trilayer graphene, where under an appropriately directed electric field the flat bands have Chern numbers ± 3 [38].

Accounting for the C_{2z}-breaking substrate, the basic structure of the problem is as follows. The gap at CN allows us to focus only on the four nearly degenerate conduction (valence) bands for fillings above (below) CN, i.e., $\nu > 0$ ($\nu < 0$). These four Chern bands are uniquely labeled by their valley $\tau = +, -$ and spin $s = \uparrow, \downarrow$; time reversal switches the valley index and enforces opposite Chern numbers for bands from opposite valleys. Since a $|C| = 1$ band is topologically equivalent to a Landau level (LL), the problem is roughly analogous to a spinful bilayer quantum Hall problem with one flux quanta per unit cell, but with opposite layers (valleys) experiencing opposite magnetic fields. The LLs are degenerate, but as in a quantum Hall ferromagnet (QHFM) [39] at integer filling the electrons may open a gap by spontaneously polarizing into a subset of these LLs, or a coherent superposition of them. In conventional quantum Hall bilayers at filling $\nu = 1$, interactions generically drive interlayer coherence, e.g., the exciton condensate [40,41]. But the twist here is the opposing Chern numbers of the two valleys. We find that the Chern number structure provides a topological reason for penalizing a coherent state: an exciton condensate between $C = 1, -1$ bands is analogous to a superconductor in a strong magnetic field, which forces vortices into the order parameter, reducing the gain in the correlation energy. Hence, a spontaneously valley-polarized (VP) state is stable and exhibits an AH effect with Hall resistance $\sim h/e^2$ (QAH if completely spin and valley polarized). Further, pinning of valley polarization by an out-of-plane B^z due to a large orbital g factor explains the presence of the R_{xy} hysteresis loop observed in Ref. [29].

The possibility of spin and valley polarization and/or quantum anomalous Hall physics and chiral edge states in

 © 2020 American Physical Society

TBG has been discussed previously in Refs. [38,42–50], albeit from a different perspective. We also note that a recent self-consistent Hartree-Fock (HF) treatment of the continuum model exhibits *spontaneous* $C_{2z}T$ breaking at CN, though the resulting Chern numbers were $C = \pm 2$ [46].

Substrate-induced Dirac mass and Chern numbers.—We model the effect of the h-BN substrate [31] by including in our band calculations a uniform but C_{2z} breaking $A - B$ sublattice splitting Δ_t and Δ_b on the top and bottom layer respectively (see the Supplemental Material [51] for details). While h-BN may also introduce a Moiré potential, its magnitude falls off much more rapidly with alignment angle than $\Delta_{t/b}$ [37]. For our calculations we used a twist angle $\theta \approx 1.05°$, and have taken a phenomenological corrugation effect into account by using a larger AB/BA interlayer hopping w_1 as compared to the AA/BB interlayer hopping w_0. Taking $w_0/w_1 = 0.85$ results in flat bands separated from the dispersing bands by an energy gap of approximately 20 meV (for zero sublattice splittings).

With sublattice splitting, the phases of the $\tau = +$ valley (or K valley of monolayer graphene) Moiré Hamiltonian for different parameter regimes of Δ_t and Δ_b are shown in Fig. 1. We find four different regions where both Dirac cones in the MBZ are gapped because of the sublattice splittings. In these regions, there are two isolated flat bands. We find that these four regions have bands with Chern numbers [59] $C = \pm 1$ or $C = 0$, and are separated from each other by a Dirac point at either the K_- or K_+ point in the MBZ. In Fig. 1 we show the Chern number of the flat band for the $\tau = +$ valley above (below) CN in green (orange). The Chern number for the flat bands from the $\tau = -$ valley can be obtained by a time reversal.

The location of the $C = \pm 1$ phases can be understood from the fact that for small $\Delta_t = \Delta_b > 0$ or $\Delta_t = \Delta_b < 0$, the leading order effect of the sublattice potentials is to generate Dirac masses with the same sign at both the K_- and K_+ points of the MBZ. Because both Dirac cones in a single valley have the same chirality, this leads to bands with Chern number ± 1, a feature earlier work dubbed a "flipped Haldane model" [60] (see also [61–63]). From Fig. 1 we see that even if only one of the layers has a nonzero sublattice splitting, the strong interlayer coupling ensures that both Dirac cones at the MBZ K points acquire a mass.These findings can also be inferred analytically within the "chiral" approximation of twisted bi-layer graphene [64,65], in which all bands are sublattice polarized and carry Chern number $C = \sigma\tau$, where σ denotes sublattice.

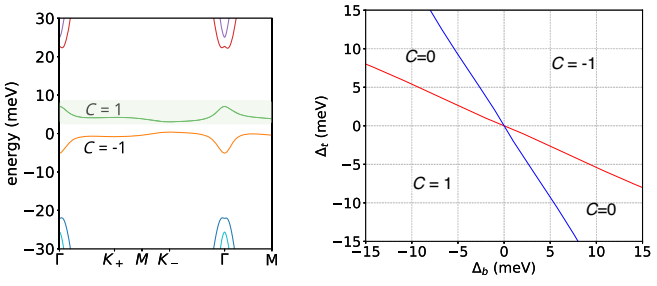

(a) (b)

FIG. 1. The effect of sublattice splittings Δ_t and Δ_b on the spinless single-valley Moiré Hamiltonian (SVMH). (a) Band structure around CN for $\Delta_t = 15$ meV and $\Delta_b = 0$. The flat band above (below) CN has Chern number $C = -1$ ($C = 1$). (b) Phase diagram of the SVMH for different Δ_t and Δ_b. Phases are labeled by the Chern number C of the flat $\tau = +$ conduction band. Blue (red) transition lines are characterized by a Dirac cone at the K_- (K_+) point of the MBZ.

Metal-valley polarization competition.—In this Letter, we focus only on the four flat *conduction* bands above the CNP (the highlighted band in Fig. 1 and its valley and spin counterparts). In the Supplemental Material, we numerically justify this for TBG, showing that $\Delta_t \sim 15$ meV ($\Delta_b = 0$) creates a 30 meV gap between valence and conduction bands [51]. To phenomenologically model the effect of interactions in this set of bands we adopt a lowest Landau level (LLL) description. We can map the Chern bands to a LLL by constructing the Wannier-Qi states [51,66,67]. In the following, we use an approximation where the Wannier-Qi states of the flat bands are replaced by the continuum LLL wave functions of a two-dimensional electron gas. Physically, this amounts to neglecting the inhomogeneous Berry curvature in the Chern bands. The AH effect and edge transport reported in Ref. [29] can be explained if there is one VP hole per Moiré unit cell. From the data in Ref. [29] is not possible to exclude a spin-unpolarized, gapless phase. If the spins do polarize however, the underlying mechanism is expected to be the same as in conventional QHFM [39], and is not sensitive to the opposite Chern numbers of the two valleys. Therefore, in the analysis below we ignore spin and focus on the mechanism of valley polarization. Considering the uniform repulsive nature of the projected Coulomb interaction and the numerical evidence against stripes in the LLL [68], we disregard the possibility of interaction-induced charge density waves, and focus on the competition between valley-polarized, intervalley coherent and metallic phases. For this we need to introduce two parameters in our LLL toy model: the bandwidth and the interaction anisotropy. To achieve a nonzero bandwidth we use a square lattice potential, that sidesteps the complexities of a hexagonal lattice and allows analytical progress.

We consider a torus of length L_x (L_y) in the x (y) direction, with a magnetic field perpendicular to the surface. We choose units in which $L_x L_y = 2\pi N_\phi l_B^2 \equiv N_\phi a^2$, where N_ϕ is the number of flux quanta piercing the torus, and $l_B = (\hbar/eB)^{-1/2}$ is the magnetic length. In particular, we will take $L_x = N_x a$ and $L_y = N_y a$, with $N_\phi = N_x N_y$. Next to the magnetic field, we also add a periodic potential $V_P(x, y) = w[\cos(2\pi x/a) + \cos(2\pi y/a)]$, such that there is exactly 2π flux in each unit cell. The potential is invariant

under translations over a in both the x and y directions, which means that the momenta $k_x = n(2\pi/N_x a)$ and $k_y = n(2\pi/N_y a)$ ($n \in \mathbb{Z}$) are good quantum numbers.

We are interested in the physics in the LLL with Chern numbers $C = 1, -1$. The electron creation operator projected in these subspaces takes the form $\psi^\dagger_\pm(x,y) = (1/\sqrt{L_y l_B \sqrt{\pi}}) \sum_k e^{iky-(1/2l_B^2)(x\mp kl_B^2)^2} c^\dagger_{\pm,k}$, where we have chosen the Landau gauge which explicitly preserves (continuous) translation symmetry in the y direction, such that $k = 2\pi n/L_y = 2\pi n/N_y a$ with $n \in \{0, 1, \ldots, N_x N_y\}$. We now proceed in analogy to Ref. [69], and define the Bloch states $c^\dagger_{\pm,(k_x,k_y)} = c^\dagger_{\pm,\mathbf{k}}$ as

$$c^\dagger_{\pm,\mathbf{k}} = \frac{1}{\sqrt{N_x}} \sum_{n=0}^{N_x-1} e^{\pm ik_x(k_y+nQ)l_B^2} c^\dagger_{\pm,k_y+nQ}, \tag{1}$$

where $Q = \sqrt{2\pi}/l_B = 2\pi/a$. The density operator in the LLL $n_\pm(\mathbf{q}) = \int d\mathbf{r} e^{-i\mathbf{q}\cdot\mathbf{r}} \psi^\dagger_\pm(\mathbf{r})\psi_\pm(\mathbf{r})$ takes the form

$$n_\pm(\mathbf{q}) = F(\mathbf{q}) \sum_{k_x,k_y} e^{\pm iq_y k_x l_B^2} c^\dagger_{\pm,\mathbf{k}-\mathbf{q}/2} c_{\pm,\mathbf{k}+\mathbf{q}/2}, \tag{2}$$

where the form factor is given by $F(\mathbf{q}) = e^{-\mathbf{q}^2 l_B^2/4}$. In the Bloch basis, the Hamiltonian term associated with the periodic potential takes the diagonal form $H^p = \sum_\mathbf{k} \varepsilon_\mathbf{k}(c^\dagger_{+,\mathbf{k}} c_{+,\mathbf{k}} + c^\dagger_{-,\mathbf{k}} c_{-,\mathbf{k}})$, with $\varepsilon_\mathbf{k} = -we^{-\pi/2}[\cos(k_x a) + \cos(k_y a)]$.

We are interested in the effect of density-density interactions on the LLL electrons moving in the periodic potential, described by the following Hamiltonian:

$$H^i = \frac{1}{2N_\phi} \sum_{\mathbf{q},\tau,\tau'} V_{\tau,\tau'}(\mathbf{q}) :n_\tau(\mathbf{q}) n_{\tau'}(-\mathbf{q}), \tag{3}$$

where we neglect the small intervalley scattering terms [51]. We will consider a general repulsive interaction of the form $V(\mathbf{q})F^2(\mathbf{q}) = u_0(\mathbf{q})(\mathbb{1} + \tau^x) + u_1(\mathbf{q})(\mathbb{1} - \tau^x)$. In analogy to quantum Hall ferromagnetism [39,40,70] and related strongly coupled systems [71,72], at the half filling of the two bands we expect that the main effect of H^i is to introduce a valley Hund's coupling between the electrons resulting in an insulating ground state. On the other hand, the *kinetic* term H^p coming from the periodic potential favors a metal over the VP insulator. To study the competition between these two phases, we perform a HF analysis using Slater determinants with correlation matrix $\langle c^\dagger_{\tau,\mathbf{k}} c_{\tau',\mathbf{k}'}\rangle = \delta_{\tau,\tau'}\delta_{\mathbf{k},\mathbf{k}'}\Theta(\epsilon_F^\tau - \epsilon_\mathbf{k})$, such that $\sum_\tau \sum_\mathbf{k} \Theta(\epsilon_F^\tau - \epsilon_\mathbf{k}) = N_\phi$. The possibility of intervalley coherent states is addressed in the next section. For each Slater determinant, we define the corresponding valley polarization P_v as $P_v = (N_+ - N_-)/N_\phi$, where N_+ (N_-) is the number of electrons in the + (−) valley. Without loss of generality, we restrict to $P_v > 0$.

We first consider an isotropic ($u_1(\mathbf{q}) = 0$) dual-gate screened Coulomb potential with LLL form factors $u_0(\mathbf{q}) = 2\pi U e^{-\mathbf{q}^2 l_B^2/2} \tanh(d|\mathbf{q}|)/|\mathbf{q}|$, and screening length $d = a$. Using this interaction potential, we calculated the HF energy E^{HF} [51]. We find that for $W/U \lesssim 0.6$, where $W \equiv 4we^{-\pi/2}$ is the bandwidth, the completely VP state indeed has the lowest energy. When $W/U \approx 0.6$, the valley polarization P_v of the optimal Slater determinant jumps and starts decreasing continuously, indicating a first-order Mott transition from the VP insulator to an itinerant valley ferromagnet. Around $W/U \approx 2.0$, P_v continuously goes to zero and a conventional metallic phase sets in the Supplemental Material [51].

Intervalley coherence and exciton vortex lattice.—In bilayer QH ferromagnets, the insulating layer-polarized state is unstable to a uniform exciton condensate or interlayer coherent state in presence of infinitesimal interaction anisotropy $u_1(\mathbf{q}) > 0$ [40]. The situation here is different as even with $u_1(\mathbf{q}) = 0$, there is no SU(2) valley symmetry because of the Chern number mismatch. The VP state therefore only breaks discrete symmetries, indicating there will be no instability of this insulating state. Another, more physical, way to understand the absence of an exciton condensation instability is to use an analogy with type II superconductors. Because electrons in bands with an opposite Chern numbers effectively see opposite magnetic fields, an electron-hole condensate $\Delta(\mathbf{r}) = \langle c^\dagger_{+,\mathbf{r}} c_{-,\mathbf{r}}\rangle$ will behave like a charge $2e$ superconducting order parameter in a perpendicular magnetic field. However, in our scenario, a Meissner-like effect, corresponding to uniform amplitude of the exciton order parameter, is ruled out from the outset. Rather, the magnetic field must leak through vortices in the exciton order parameter, leading to an excitonic vortex lattice phase. In this section, we show that both the VP insulator and the unpolarized metal are energetically favorable to the exciton vortex lattice, for sufficiently small interaction anisotropy $u_1(\mathbf{q})$.

For our LLL model, we can derive an exact expression for the exciton vortex lattice order parameter $\Delta(\mathbf{r})$. To respect all symmetries of the square lattice, we expect $\Delta(\mathbf{r})$ to have vortices at both the lattice sites and the plaquette centers, leading to a 4π vorticity in each unit cell. In the analytically tractable limit, we can uniquely determine $\Delta(\mathbf{r})$ up to a translation by demanding its invariance under the magnetic translations $\mathcal{T}(a\hat{x})$ and $\mathcal{T}(a/2(\hat{x}+\hat{y}))$, connecting the anticipated vortices [51]. In Fig. 2 we plot the magnitude of $\Delta(\mathbf{r})$ thus obtained, from which we clearly see the expected Abrikosov vortex lattice. Projecting $\Delta(\mathbf{r})$ to the LLL Bloch basis wave functions $\phi_{\pm,\mathbf{k}}(\mathbf{r})$ leads to a diagonal order parameter

$$\Delta_\mathbf{k} = \Delta_0 \sum_{j=-\infty}^{\infty} e^{-i(\pi/2)j^2} e^{-1/4(2k_y+jQ)^2 l_B^2 - ik_x(2k_y+jQ)l_B^2}, \tag{4}$$

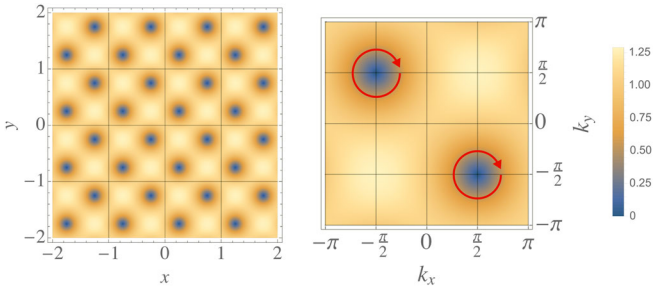

FIG. 2. The magnitude of the excitonic order parameter in real (left) and momentum (right) space (for $a = 1$, $\Delta_0 = 1$). The red circles denote identical phase winding of $\Delta_{\mathbf{k}}$ at both nodal points.

where Δ_0 represents the overall strength of the exciton condensate. $\Delta_{\mathbf{k}}$ has two nodes with identical phase winding at $\mathbf{k} = \pm(\pi/2, -\pi/2)$, as shown in Fig. 2 [51].

The presence of two zeros in the BZ with the same phase winding is a topological *requirement* for the exciton order parameter, and is not an artifact of our effective LLL model. In an isolated band a with nonzero Chern number C_a, the phase of the electron creation operator $c^\dagger_{a,\mathbf{k}}$ cannot be chosen to be both continuous and single-valued over the BZ. In particular, it must wind $2\pi C_a$ times along the boundary of the BZ in a continuous gauge choice. This implies that the phase of $\Delta_{\mathbf{k}} = \langle c^\dagger_{+,\mathbf{k}} c_{-,\mathbf{k}} \rangle$ winds $2\pi(C_a - C_b) = 4\pi$ times along the BZ boundary for bands from opposite valleys with $C_a = 1$ and $C_b = -1$, which precisely corresponds to winding around two zeros with identical chirality.

We now demonstrate that variational states with an exciton vortex lattice have higher energy than the VP state or the metal for small anisotropy u_1 in the interaction H^i. We consider the Slater determinant ground state $|\psi_{\mathrm{MF}}\rangle$ of the mean-field Hamiltonian $H_{\mathrm{MF}} = \sum_{\mathbf{k},\tau,\tau'} c^\dagger_{\mathbf{k},\tau} h_{\tau,\tau'}(\mathbf{k}) c_{\mathbf{k},\tau'}$, where $h_{\tau,\tau'}(\mathbf{k}) = \epsilon_{\mathbf{k}} \mathbb{1} + h\tau^z + \mathrm{Re}(\Delta_{\mathbf{k}})\tau^x + \mathrm{Im}(\Delta_{\mathbf{k}})\tau^y$. $|\psi_{\mathrm{MF}}\rangle$ is characterized by the valley polarization P_v (determined by h) and an exciton vortex lattice of strength Δ_0, to be treated as variational parameters. The correlation matrix evaluated in this state takes the form of the projector $\langle c^\dagger_{\tau,\mathbf{k}} c_{\tau'\mathbf{k}'} \rangle = P_{\tau,\tau'}(\mathbf{k}) \delta_{\mathbf{k},\mathbf{k}'}$, which can be used to evaluate the regularized HF energy density $e^{\mathrm{HF}}(P_v, \Delta_0)$ of the variational state for a given microscopic interaction at a fixed filling $\nu = 1$. We find that the global minimum of e^{HF} lies at $|P_v| = 1$ and $\Delta_0 = 0$ for the insulator in the limit of flat bands and isotropic interaction ($u_1 = 0$) [51]. We next show that the states of interest, with a fixed valley polarization P_v at filling $\nu = 1$, are stable to the formation of an vortex lattice in presence of small interaction anisotropy. To do this, we consider the difference in energy density $e^{\mathrm{HF}}(P_v, \Delta_0) - e^{\mathrm{HF}}(P_v, 0)$ perturbatively in $|\Delta_0|$ for arbitrary repulsive interaction parametrized by u_0 and u_1; a positive difference would indicate that $\Delta_0 = 0$ corresponds to an energy minimum. For the polarized phase, we find

$$e^{\mathrm{HF}}(1, \Delta_0) - e^{\mathrm{HF}}(1, 0) = \frac{1}{8h^2}\left[\int_{\mathbf{k},\mathbf{q}} u_0(\mathbf{q})|\Delta_+ - \Delta_-|^2 + \int_{\mathbf{k},\mathbf{q}} u_1(\mathbf{q})|\Delta_+ + \Delta_-|^2 - 4u_1(\mathbf{0}) \int_{\mathbf{k}} |\Delta_{\mathbf{k}}|^2\right], \quad (5)$$

where $\Delta_\pm \equiv \Delta_{\mathbf{k}\pm\mathbf{q}/2}$ [51]. For a uniform exciton condensate, $\Delta_{\mathbf{k}} = \Delta_0$ and this energy difference is negative [51]. However, for an exciton order parameter formed with electrons and holes from opposite Chern bands, $\nabla_{\mathbf{k}} \Delta_{\mathbf{k}} \neq 0$. Therefore, when u_1 is sufficiently small compared to u_0, the energy of the state with nonzero $\Delta_{\mathbf{k}}$ is higher. So the VP state with $\Delta_0 = 0$, previously shown to be the ground state with an isotropic interaction for small W/u_0, is indeed robust to small interaction anisotropy. Analogous computations [51] show that the unpolarized metal ($P_v = 0 = \Delta_0$) is stable to the vortex lattice as well. An approximate phase diagram of our model for a short-range (LLL-projected) interaction anisotropy $u_1(\mathbf{q}) = u_1 e^{-\mathbf{q}^2 l_B^2/2}$ is presented in Fig. 3. For TBG, we expect $W/U \lesssim 0.2$ from the ratio of the bandwidth to the Coulomb interaction, and the anisotropy $u_1/U \lesssim 0.01$ to be small [51,73], indicating a VP phase consistent with experiments [29,74]. In the supplement, we numerically solve the mean-field equations for TBG on h-BN at $\nu = 3$ and confirm that the spin and VP QAH state is indeed the ground state.

Valley-Zeeman effect.—Having argued in favor of a VP state at $\nu = 3$, we turn to the observed hysteresis in the $\nu = 3$ Hall conductance as a function of out-of-plane magnetic field B^z [29]. To this end, we compute the orbital g_v-factor for the TBG conduction bands. In a band τ without time-reversal electrons can carry a momentum-dependent orbital moment $m_{\tau,\mathbf{k}}$ [75,76]. Time reversal ensures that $m_{\tau,\mathbf{k}} = -m_{-\tau,-\mathbf{k}}$, which averaged over the MBZ produces a valley-Zeeman splitting $E = -g_v(\tau^z/2)\mu_B B^z$. We find that for $\Delta_b = 0$, $\Delta_t \sim 10$–30 meV, g_v ranges from approximately -2 to -6 [51]. Note that for $B^z > 0$, the $C = 1$

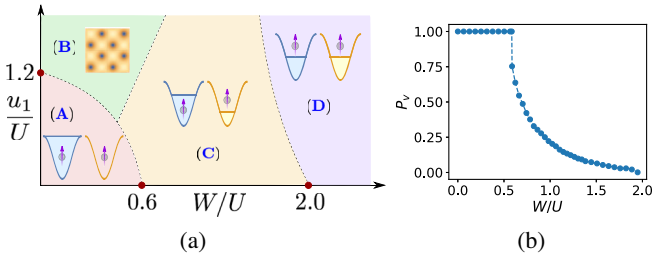

FIG. 3. (a) Approximate phase diagram of spin-polarized interacting electrons from opposite valleys in $C = \pm 1$ bands. The phases are (A) fully VP insulator, (B) exciton vortex lattice, (C) partially polarized metal or itinerant valley ferromagnet, and (D) unpolarized metal. Everywhere within phases A and C, $R_{xy} \neq 0$. (b) Metal-insulator competition and the valley polarization P_v for isotropic interaction.

band comes down in energy. The sign of this effect is in agreement with the Landau fans of Refs. [29,74].

Conclusion.—We showed that broken inversion symmetry in TBG due to substrate (h-BN) coupling leads to two Chern bands per valley. Spontaneous polarization of holes in spin and valley space then leads to an AH state at $\nu = 3$. Using a LLL model, a HF analysis establishes a stable VP state as the ground state when the bandwidth is small compared to the interaction strength. The opposite Chern numbers for the two valleys precludes uniform intervalley coherence. The resultant exciton vortex lattice structure reduces correlation energy gain and stabilizes valley polarization. This result agrees with numerical work on a Hubbard model [77].

We thank Aaron Sharpe, Eli Fox, and David Goldhaber-Gordon for discussions about their data and sharing their insights. We also thank Ryan Mishmash for explaining the details of Ref. [69] to two of us (S. C. and N. B.), and Ehud Altman, Senthil Todadri, and Andrea Young for inspiring discussions. Our work overlaps with concurrent work by Y. Zhang, D. Mao, and T. Senthil [78]. M. Z. and N. B. were supported by the DOE, office of Basic Energy Sciences under Contract No. DE-AC02-05-CH11231. S. C. acknowledges support from the ERC synergy grant UQUAM via E. Altman.

Note added.—Recently, a quantized AHE with net Chern number $C = 1$ has been observed for a gapped insulator at $\nu = 3$ in TBG aligned with h-BN [74], consistent with our theoretical results. Quantized AHE arising from valley-Chern bands have also been observed [79] and proposed [80,81] in other Moiré heterostructures, in accordance with our phenomenological picture of interaction in nearly flat bands with opposite Chern numbers.

*N. B. and S. C. contributed equally to this work.

[1] A. K. Geim and I. V. Grigorieva, Van der waals heterostructures, Nature (London) **499**, 419 (2013).
[2] R. Bistritzer and A. H. MacDonald, Moiré bands in twisted double-layer graphene, Proc. Natl. Acad. Sci. U.S.A. **108**, 12233 (2011).
[3] E. J. Mele, Commensuration and interlayer coherence in twisted bilayer graphene, Phys. Rev. B **81**, 161405(R) (2010).
[4] J. M. B. Lopes dos Santos, N. M. R. Peres, and A. H. Castro Neto, Continuum model of the twisted graphene bilayer, Phys. Rev. B **86**, 155449 (2012).
[5] J. M. B. Lopes dos Santos, N. M. R. Peres, and A. H. Castro Neto, Graphene Bilayer With a Twist: Electronic Structure, Phys. Rev. Lett. **99**, 256802 (2007).
[6] G. Trambly de Laissardière, D. Mayou, and L. Magaud, Localization of dirac electrons in rotated graphene bilayers, Nano Lett. **10**, 804 (2010).
[7] S. Shallcross, S. Sharma, E. Kandelaki, and O. A. Pankratov, Electronic structure of turbostratic graphene, Phys. Rev. B **81**, 165105 (2010).
[8] E. Suárez Morell, J. D. Correa, P. Vargas, M. Pacheco, and Z. Barticevic, Flat bands in slightly twisted bilayer graphene: Tight-binding calculations, Phys. Rev. B **82**, 121407 (R) (2010).
[9] P. Moon and M. Koshino, Energy spectrum and quantum hall effect in twisted bilayer graphene, Phys. Rev. B **85**, 195458 (2012).
[10] G. Li, A. Luican, J. M. B. Lopes dos Santos, A. H. Castro Neto, A. Reina, J. Kong, and E. Y. Andrei, Observation of van hove singularities in twisted graphene layers, Nat. Phys. **6**, 109 (2010).
[11] A. Luican, G. Li, A. Reina, J. Kong, R. R. Nair, K. S. Novoselov, A. K. Geim, and E. Y. Andrei, Single-Layer Behavior and Its Breakdown in Twisted Graphene Layers, Phys. Rev. Lett. **106**, 126802 (2011).
[12] W. Yan, M. Liu, R.-F. Dou, L. Meng, L. Feng, Z.-D. Chu, Y. Zhang, Z. Liu, J.-C. Nie, and L. He, Angle-Dependent Van Hove Singularities in a Slightly Twisted Graphene Bilayer, Phys. Rev. Lett. **109**, 126801 (2012).
[13] I. Brihuega, P. Mallet, H. González-Herrero, G. Trambly de Laissardière, M. M. Ugeda, L. Magaud, J. M. Gómez-Rodríguez, F. Ynduráin, and J.-Y. Veuillen, Unraveling the Intrinsic and Robust Nature of Van Hove Singularities in Twisted Bilayer Graphene by Scanning Tunneling Microscopy and Theoretical Analysis, Phys. Rev. Lett. **109**, 196802 (2012).
[14] T. Ohta, J. T. Robinson, P. J. Feibelman, A. Bostwick, E. Rotenberg, and T. E. Beechem, Evidence for Interlayer Coupling and Moiré Periodic Potentials in Twisted Bilayer Graphene, Phys. Rev. Lett. **109**, 186807 (2012).
[15] R. W. Havener, Y. Liang, L. Brown, L. Yang, and J. Park, Van hove singularities and excitonic effects in the optical conductivity of twisted bilayer graphene, Nano Lett. **14**, 3353 (2014).
[16] R. de Gail, M. O. Goerbig, F. Guinea, G. Montambaux, and A. H. Castro Neto, Topologically protected zero modes in twisted bilayer graphene, Phys. Rev. B **84**, 045436 (2011).
[17] K. Uchida, S. Furuya, J.-I. Iwata, and A. Oshiyama, Atomic corrugation and electron localization due to moiré patterns in twisted bilayer graphenes, Phys. Rev. B **90**, 155451 (2014).
[18] A. O. Sboychakov, A. L. Rakhmanov, A. V. Rozhkov, and Franco Nori, Electronic spectrum of twisted bilayer graphene, Phys. Rev. B **92**, 075402 (2015).
[19] J. Jung, A. Raoux, Z. Qiao, and A. H. MacDonald, Ab initio theory of Moiré superlattice bands in layered two-dimensional materials, Phys. Rev. B **89**, 205414 (2014).
[20] D. Wong, Y. Wang, J. Jung, S. Pezzini, A. M. DaSilva, H.-Z. Tsai, H. S. Jung, R. Khajeh, Y. Kim, J. Lee, S. Kahn, S. Tollabimazraehno, H. Rasool, K. Watanabe, T. Taniguchi, A. Zettl, S. Adam, A. H. MacDonald, and M. F. Crommie, Local spectroscopy of Moiré-induced electronic structure in gate-tunable twisted bilayer graphene, Phys. Rev. B **92**, 155409 (2015).
[21] S. Fang and E. Kaxiras, Electronic structure theory of weakly interacting bilayers, Phys. Rev. B **93**, 235153 (2016).

[22] Y. Cao, J. Y. Luo, V. Fatemi, S. Fang, J. D. Sanchez-Yamagishi, K. Watanabe, T. Taniguchi, E. Kaxiras, and P. Jarillo-Herrero, Superlattice-Induced Insulating States and Valley-Protected Orbits in Twisted Bilayer Graphene, Phys. Rev. Lett. **117**, 116804 (2016).

[23] K. Kim, A. DaSilva, S. Huang, B. Fallahazad, S. Larentis, T. Taniguchi, K. Watanabe, B. J. LeRoy, A. H. MacDonald, and E. Tutuc, Tunable Moiré bands and strong correlations in small-twist-angle bilayer graphene, Proc. Natl. Acad. Sci. U.S.A. **114**, 3364 (2017).

[24] Y. Cao, V. Fatemi, A. Demir, S. Fang, S. L. Tomarken, J. Y. Luo, J. D. Sanchez-Yamagishi, K. Watanabe, T. Taniguchi, E. Kaxiras, R. C. Ashoori, and P. Jarillo-Herrero, Correlated insulator behaviour at half-filling in magic-angle graphene superlattices, Nature (London) **556**, 80 (2018).

[25] M. Yankowitz, S. Chen, H. Polshyn, K. Watanabe, T. Taniguchi, D. Graf, A. F. Young, and C. R. Dean, Tuning superconductivity in twisted bilayer graphene, Science **363**, 1059 (2019).

[26] A. Kerelsky, L. McGilly, D. M. Kennes, L. Xian, M. Yankowitz, S. Chen, K. Watanabe, T. Taniguchi, J. Hone, C. Dean, A. Rubio, and A. N. Pasupathy, Magic angle spectroscopy, Nature (London) **572**, 95 (2019).

[27] Y. Choi, J. Kemmer, Y. Peng, A. Thomson, H. Arora, R. Polski, Y. Zhang, H. Ren, J. Alicea, G. Refael, F. von Oppen, K. Watanabe, T. Taniguchi, and S. Nadj-Perge, Imaging electronic correlations in twisted bilayer graphene near the magic angle, Nat. Phys. **15**, 1174 (2019).

[28] G. Chen, L. Jiang, S. Wu, B. Lv, H. Li, K. Watanabe, T. Taniguchi, Z. Shi, Y. Zhang, and F. Wang, Gate-tunable Mott insulator in trilayer graphene-boron nitride Moiré superlattice, Nat. Phys. **15**, 237 (2019).

[29] A. L. Sharpe, E. J. Fox, A. W. Barnard, J. Finney, K. Watanabe, T. Taniguchi, M. A. Kastner, and D. Goldhaber-Gordon, Emergent ferromagnetism near three-quarters filling in twisted bilayer graphene, Science **365**, 605 (2019).

[30] D. Efetov, Cascade of superconducting domes and magnetic order around quarter filling in magic angle bilayer graphene, KITP program "Correlations in Moire Flat Bands", 2019.

[31] J. Jung, A. M. DaSilva, A. H. MacDonald, and S. Adam, Origin of band gaps in graphene on hexagonal boron nitride, Nat. Commun. **6**, 6308 (2015).

[32] B. Hunt, J. D. Sanchez-Yamagishi, A. F. Young, M. Yankowitz, B. J. LeRoy, K. Watanabe, T. Taniguchi, P. Moon, M. Koshino, P. Jarillo- Herrero, and R. C. Ashoori, Massive Dirac fermions and Hofstadter butterfly in a van der Waals heterostructure, Science **340**, 1427 (2013).

[33] F. Amet, J. R. Williams, K. Watanabe, T. Taniguchi, and D. Goldhaber-Gordon, Insulating Behavior at the Neutrality Point in Single-Layer Graphene, Phys. Rev. Lett. **110**, 216601 (2013).

[34] M. Lee, J. R. Wallbank, P. Gallagher, K. Watanabe, T. Taniguchi, V. I. Fal'ko, and D. Goldhaber-Gordon, Ballistic miniband conduction in a graphene superlattice, Science **353**, 1526 (2016).

[35] M. Yankowitz, J. Jung, E. Laksono, N. Leconte, B. L. Chittari, K. Watanabe, T. Taniguchi, S. Adam, D. Graf, and C. R. Dean, Dynamic band-structure tuning of graphene Moiré superlattices with pressure, Nature (London) **557**, 404 (2018).

[36] A. A. Zibrov, E. M. Spanton, H. Zhou, C. Kometter, T. Taniguchi, K. Watanabe, and A. F. Young, Even-denominator fractional quantum Hall states at an isospin transition in monolayer graphene, Nat. Phys. **14**, 930 (2018).

[37] H. Kim, N. Leconte, B. L. Chittari, K. Watanabe, T. Taniguchi, A. H. MacDonald, J. Jung, and S. Jung, Accurate gap determination in monolayer and bilayer graphene/h-BN Moiré superlattices, Nano Lett. **18**, 7732 (2018).

[38] Y.-H. Zhang, D. Mao, Y. Cao, P. Jarillo-Herrero, and T. Senthil, Nearly flat Chern bands in Moiré superlattices, Phys. Rev. B **99**, 075127 (2019).

[39] S. L. Sondhi, A. Karlhede, S. A. Kivelson, and E. H. Rezayi, Skyrmions and the crossover from the integer to fractional quantum hall effect at small zeeman energies, Phys. Rev. B **47**, 16419 (1993).

[40] J. P. Eisenstein, Exciton condensation in bilayer quantum hall systems, Annu. Rev. Condens. Matter Phys. **5**, 159 (2014).

[41] E. Tutuc, M. Shayegan, and D. A. Huse, Counterflow Measurements in Strongly Correlated GaAs Hole Bilayers: Evidence for Electron-Hole Pairing, Phys. Rev. Lett. **93**, 036802 (2004).

[42] J. F. Dodaro, S. A. Kivelson, Y. Schattner, X. Q. Sun, and C. Wang, Phases of a phenomenological model of twisted bilayer graphene, Phys. Rev. B **98**, 075154 (2018).

[43] A. Thomson, S. Chatterjee, S. Sachdev, and M. S. Scheurer, Triangular antiferromagnetism on the honeycomb lattice of twisted bilayer graphene, Phys. Rev. B **98**, 075109 (2018).

[44] J. Kang and O. Vafek, Strong Coupling Phases of Partially Filled Twisted Bilayer Graphene Narrow Bands, Phys. Rev. Lett. **122**, 246401 (2019).

[45] M. Ochi, M. Koshino, and K. Kuroki, Possible correlated insulating states in magic-angle twisted bilayer graphene under strongly competing interactions, Phys. Rev. B **98**, 081102(R) (2018).

[46] M. Xie and A. H. MacDonald, On the Nature of the Correlated Insulator States in Twisted Bilayer Graphene, Phys. Rev. Lett. **124**, 097601 (2020).

[47] C. Xu and L. Balents, Topological Superconductivity in Twisted Multilayer Graphene, Phys. Rev. Lett. **121**, 087001 (2018).

[48] Y.-P. Lin and R. M. Nandkishore, A chiral twist on the high-T_c phase diagram in Moiré heterostructures, Phys. Rev. B **100**, 085136 (2019).

[49] J. Liu, J. Liu, and X. Dai, A complete picture for the band topology in twisted bilayer graphene, Phys. Rev. B **99**, 155415 (2019).

[50] Y.-H. Zhang and T. Senthil, Bridging Hubbard model physics and quantum Hall physics in trilayer graphene/h-BN Moiré superlattice, Phys. Rev. B **99**, 205150 (2019).

[51] See the Supplemental Material at http://link.aps.org/supplemental/10.1103/PhysRevLett.124.166601 for additional details about the band structure and mean-field calculations, which contains Refs. [52–58].

[52] D. J. Thouless, Wannier functions for magnetic sub-bands, J. Phys. C **17**, L325 (1984).

[53] R. Resta, Theory of the electric polarization in crystals, Ferroelectrics **136**, 51 (1992).

[54] R. D. King-Smith and D. Vanderbilt, Theory of polarization of crystalline solids, Phys. Rev. B **47**, 1651 (1993).
[55] N. F. Q. Yuan and L. Fu, Model for the metal-insulator transition in graphene superlattices and beyond, Phys. Rev. B **98**, 045103 (2018).
[56] J. Kang and O. Vafek, Symmetry, Maximally Localized Wannier States, and a Low-Energy Model for Twisted Bilayer Graphene Narrow Bands, Phys. Rev. X **8**, 031088 (2018).
[57] M. Koshino, N. F. Q. Yuan, T. Koretsune, M. Ochi, K. Kuroki, and L. Fu, Maximally Localized Wannier Orbitals and the Extended Hubbard Model for Twisted Bilayer Graphene, Phys. Rev. X **8**, 031087 (2018).
[58] N. Bultinck, E. Khalaf, S. Liu, S. Chatterjee, A. Vishwanath, and M. P. Zaletel, Ground state and hidden symmetry of magic angle graphene at even integer filling, arXiv:1911.02045.
[59] T. Fukui, Y. Hatsugai, and H. Suzuki, Chern numbers in discretized Brillouin zone: Efficient method of computing (spin) Hall conductances, J. Phys. Soc. Jpn. **74**, 1674 (2005).
[60] L. Zou, H. C. Po, A. Vishwanath, and T. Senthil, Band structure of twisted bilayer graphene: Emergent symmetries, commensurate approximants, and Wannier obstructions, Phys. Rev. B **98**, 085435 (2018).
[61] H. C. Po, L. Zou, A. Vishwanath, and T. Senthil, Origin of Mott Insulating Behavior and Superconductivity in Twisted Bilayer Graphene, Phys. Rev. X **8**, 031089 (2018).
[62] H. C. Po, L. Zou, T. Senthil, and A. Vishwanath, Faithful tight-binding models and fragile topology of magic-angle bilayer graphene, Phys. Rev. B **99**, 195455 (2019).
[63] Z. Song, Z. Wang, W. Shi, G. Li, C. Fang, and B. A. Bernevig, All "Magic Angles" Are "Stable" Topological, Phys. Rev. Lett. **123**, 036401 (2019).
[64] P. San-Jose, J. González, and F. Guinea, Non-Abelian Gauge Potentials in Graphene Bilayers, Phys. Rev. Lett. **108**, 216802 (2012).
[65] G. Tarnopolsky, A. J. Kruchkov, and A. Vishwanath, Origin of Magic Angles in Twisted Bilayer Graphene, Phys. Rev. Lett. **122**, 106405 (2019).
[66] N. Marzari, A. A. Mostofi, J. R. Yates, I. Souza, and D. Vanderbilt, Maximally localized Wannier functions: Theory and applications, Rev. Mod. Phys. **84**, 1419 (2012).
[67] X.-L. Qi, Generic Wave-Function Description of Fractional Quantum Anomalous Hall States and Fractional Topological Insulators, Phys. Rev. Lett. **107**, 126803 (2011).
[68] N. Shibata and D. Yoshioka, Stripe state in the lowest Landau level, J. Phys. Soc. Jpn. **73**, 1 (2004).
[69] R. V. Mishmash, A. Yazdani, and M. P. Zaletel, Majorana lattices from the quantized Hall limit of a proximitized spin-orbit coupled electron gas, Phys. Rev. B **99**, 115427 (2019).
[70] Z. F. Ezawa and G. Tsitsishvili, Quantum hall ferromagnets, Rep. Prog. Phys. **72**, 086502 (2009).
[71] T. Neupert, L. Santos, S. Ryu, C. Chamon, and C. Mudry, Topological Hubbard Model and Its High-Temperature Quantum Hall Effect, Phys. Rev. Lett. **108**, 046806 (2012).
[72] T. Neupert, L. Santos, S. Ryu, C. Chamon, and C. Mudry, Fractional topological liquids with time-reversal symmetry and their lattice realization, Phys. Rev. B **84**, 165107 (2011).
[73] S. Chatterjee, N. Bultinck, and M. P. Zaletel, Symmetry breaking and skyrmionic transport in twisted bilayer graphene, arXiv:1908.00986.
[74] M. Serlin, C. L. Tschirhart, H. Polshyn, Y. Zhang, J. Zhu, K. Watanabe, T. Taniguchi, L. Balents, and A. F. Young, Intrinsic quantized anomalous Hall effect in a Moiré heterostructure, arXiv:1907.00261.
[75] D. Xiao, M.-C. Chang, and Q. Niu, Berry phase effects on electronic properties, Rev. Mod. Phys. **82**, 1959 (2010).
[76] M.-C. Chang and Q. Niu, Berry phase, hyperorbits, and the Hofstadter spectrum: Semiclassical dynamics in magnetic bloch bands, Phys. Rev. B **53**, 7010 (1996).
[77] T. Neupert, L. Santos, S. Ryu, C. Chamon, and C. Mudry, Topological Hubbard Model and Its High-Temperature Quantum Hall Effect, Phys. Rev. Lett. **108**, 046806 (2012).
[78] Y.-H. Zhang, D. Mao, and T. Senthil, Twisted bilayer graphene aligned with hexagonal boron nitride: Anomalous hall effect and a lattice model, Nat. Commun. **10**, 5333 (2019).
[79] G. Chen, A. L. Sharpe, E. J. Fox, Y.-H. Zhang, S. Wang, L. Jiang, B. Lyu, H. Li, K. Watanabe, and T. Taniguchi, Tunable correlated Chern insulator and ferromagnetism in trilayer graphene/boron nitride Moiré superlattice, arXiv:1905.06535.
[80] X. Liu, Z. Hao, E. Khalaf, J. Y. Lee, K. Watanabe, T. Taniguchi, A. Vishwanath, and P. Kim, Spin-polarized correlated insulator and superconductor in twisted double bilayer graphene, arXiv:1903.08130.
[81] J. Y. Lee, E. Khalaf, S. Liu, X. Liu, Z. Hao, P. Kim, and A. Vishwanath, Theory of correlated insulating behaviour and spin-triplet superconductivity in twisted double bilayer graphene, Nat. Commun. **10**, 5333 (2019).